

1 **A blue-shifted genetically encoded Ca²⁺ indicator with** 2 **enhanced two-photon absorption**

3 Abhi Aggarwal^{1,4}, Smrithi Sunil^{2,†}, Imane Bendifallah^{5,†}, Michael Moon¹, Mikhail Drobizhev⁶,
4 Landon Zarowny¹, Jihong Zheng³, Sheng-Yi Wu¹, Alexander W. Lohman⁴, Alison G. Tebo³,
5 Valentina Emiliani⁵, Kaspar Podgorski^{2,3}, Yi Shen^{1*}, and Robert E. Campbell^{1,7,8*}

6
7 1. University of Alberta, Department of Chemistry, Edmonton, Alberta, Canada

8 2. Allen Institute for Neural Dynamics, Seattle, Washington, United States of America

9 3. Howard Hughes Medical Institute, Janelia Research Campus, Ashburn, Virginia,
10 United States of America.

11 4. University of Calgary, Department of Cell Biology and Anatomy and Hotchkiss Brain
12 Institute, Calgary, Alberta, Canada

13 5. Vision Institute, Sorbonne University, CNRS, INSERM, Paris, France.

14 6. Montana State University, Department of Microbiology and Cell Biology, Bozeman,
15 Montana, United States of America

16 7. Université Laval, CERVO Brain Research Center and Department of Biochemistry,
17 Microbiology, and Bioinformatics, Québec, Québec, Canada

18 8. The University of Tokyo, Department of Chemistry, Bunkyo-ku, Tokyo, Japan

19 * Correspondence should be addressed to Y.S. (yi.shen@ualberta.ca) or R.E.C.
20 (campbell@chem.s.u-tokyo.ac.jp)

21 † Equal contribution

22

23 **ABSTRACT**

24 **Significance:** Genetically encoded calcium ion (Ca^{2+}) indicators (GECIs) are powerful
25 tools for monitoring intracellular Ca^{2+} concentration changes in living cells and model
26 organisms. In particular, GECIs have found particular utility for monitoring the transient
27 increase of Ca^{2+} concentration that is associated with the neuronal action potential.
28 However, the palette of highly optimized GECIs for imaging of neuronal activity remains
29 relatively limited. Expanding the selection of available GECIs to include new colors and
30 distinct photophysical properties could create new opportunities for *in vitro* and *in vivo*
31 fluorescence imaging of neuronal activity. In particular, blue-shifted variants of GECIs are
32 expected to have enhanced two-photon brightness, which would facilitate multiphoton
33 microscopy.

34 **Aim:** We describe the development and applications of T-GECO1 – a high-performance
35 blue-shifted GECI based on the *Clavularia sp.*-derived mTFP1.

36 **Approach:** We used protein engineering and extensive directed evolution to develop T-
37 GECO1. We characterize the purified protein and assess its performance *in vitro* using
38 one-photon excitation in cultured rat hippocampal neurons, *in vivo* using one-photon
39 excitation fiber photometry in mice, and *ex vivo* using two-photon Ca^{2+} imaging in
40 hippocampal slices.

41 **Results:** The Ca^{2+} -bound state of T-GECO1 has an excitation peak maximum of 468 nm,
42 an emission peak maximum of 500 nm, an extinction coefficient of $49,300 \text{ M}^{-1}\text{cm}^{-1}$, a
43 quantum yield of 0.83, and two-photon brightness approximately double that of EGFP.
44 The Ca^{2+} -dependent fluorescence increase is 15-fold and the apparent K_d for Ca^{2+} is 82
45 nM. With two-photon excitation conditions at 850 nm, T-GECO1 consistently enabled

46 detection of action potentials with higher signal-to-noise (SNR) than a late generation
47 GCaMP variant.

48 **Conclusion:** T-GECO1 is a high performance blue-shifted GECI that, under two-photon
49 excitation conditions, provides advantages relative to late generation GCaMP variants.

50 **Keywords:** genetically encoded calcium ion indicator; protein engineering; blue-shifted
51 fluorescence; neuronal activity imaging; two-photon excitation.

52

53 **1 Introduction**

54 Genetically encodable calcium ion (Ca^{2+}) indicators (GECIs), engineered from *Aequorea victoria*
55 green fluorescent protein (avGFP),¹ or its homologs, are powerful tools for enabling observation
56 of intracellular Ca^{2+} dynamics. Among GECIs, the highly optimized jGCaMP series represents the
57 tip of the spear with respect to pushing the limits of *in vivo* performance, particularly for the
58 imaging of neural activity.²⁻⁴

59 The jGCaMP series has been iteratively and aggressively optimized for high sensitivity, high
60 brightness under one-photon excitation, and fast kinetics, to great success.⁴ However, there are a
61 variety of other desirable GECI properties that are unlikely to be realized with the avGFP-derived
62 jGCaMP series, regardless of the extent of optimization. Such properties tend to be those that are
63 intrinsic to the parent fluorescent protein (FP), such as higher two-photon brightness, fluorescence
64 hues other than green, or the ability to be photoconverted. To obtain GECIs with these properties,
65 it is generally necessary to undertake the labor-intensive re-engineering of a new GECI, starting
66 from a new parent FP. Notable examples of such efforts include the development of GECIs that
67 are mNeonGreen-derived,^{5,6} yellow fluorescent,^{7,8} red fluorescent,⁹⁻¹¹ near-infrared
68 fluorescent,^{12,13} or photoconvertible.¹⁴⁻¹⁶

69 One GECI feature that has remained under-explored is blue-shifted excitation and emission.
70 Blue-shifted GECIs with anionic chromophore are expected to be much brighter under two-photon
71 excitation¹⁷ which could enable Ca²⁺ imaging with increased sensitivity. Furthermore, blue-shifted
72 GECIs could be preferred relative to green fluorescent GECIs for applications that combine two-
73 photon activation of opsin-based optogenetic actuators and Ca²⁺ imaging. There is strong overlap
74 of the two-photon spectrum of GCaMPs with the spectra of the most commonly used opsin-based
75 optogenetic actuators, and so there is inevitably unwanted optogenetic activation during Ca²⁺
76 imaging. In principle, a blue-shifted GECI, with effective two-photon excitation at ~800 nm,
77 would circumvent this problem. It must be noted that a blue-shifted GECI with performance
78 comparable to a recent generation GCaMP, would still have some inherent disadvantages, such as
79 reduced working depth, due to increased scattering of blue-shifted light when it passes through
80 tissue.

81 Previous efforts to develop blue-shifted GECIs have relied on the same strategy that was
82 originally used to convert avGFP in a blue FP (BFP) – mutation of the tyrosine residue in the
83 chromophore forming tripeptide to histidine (Y66H).¹⁸ For example, B-GECO1,⁹ BCaMP1,¹⁹ and
84 X-CaMP-B,²⁰ are blue fluorescent GECIs that were created using this strategy. Unfortunately,
85 these blue fluorescent GECIs suffer from substantially lower sensitivity and lower brightness,
86 relative to optimized GCaMP variants. A blue-shifted Ca²⁺ indicator optimized for Ca²⁺-dependent
87 change in fluorescence lifetime, with a tryptophan-derived chromophore (Y67W), has also been
88 reported.²¹

89 In contrast to the engineered BFPs with the Y67H mutation, there are naturally occurring blue-
90 shifted FPs that retain a tyrosine-derived chromophore.²² One such FP is the tetrameric cFP484
91 cyan FP (CFP) from *Clavularia sp.*, which was engineered to give the monomeric teal fluorescent

92 protein 1 (mTFP1).²³ mTFP1 (excitation maximum 462 nm, emission maximum 492 nm) is blue-
93 shifted and 1.6× brighter, relative to avGFP-derived EGFP (excitation maximum 488 nm, emission
94 maximum 508 nm).^{1,24} Molina et al. have demonstrated that blue-shifted FPs with tyrosine-derived
95 chromophores are substantially brighter than EGFP under two-photon excitation.¹⁷ The promising
96 properties of the mTFP1 parent protein inspired us to attempt to create a new GECI based on this
97 scaffold. Precedent for this effort comes from the successful development of mTFP1-based
98 genetically encoded Zn²⁺ indicators.²⁵

99 In this work, we take advantage of the mTFP1 parent protein to develop a novel GECI named
100 T-GECO1. By capitalizing on the unique spectral properties and high two-photon cross-section of
101 mTFP1, T-GECO1 expands the possibilities for Ca²⁺ imaging experiments and opens new avenues
102 for measuring intracellular Ca²⁺, enabling spectral advantages, compatibility with multiplexing
103 and all-optical experiments, and provides higher two-photon cross-section for enhanced
104 performance *in vitro* and *in vivo*. Here, we present the design, optimization, and characterization
105 of T-GECO1 in soluble protein, cultured neurons, organotypic hippocampal slices, and *in vivo*.

106 **2 Methods**

107 **2.1 Molecular biology and protein engineering**

108 To develop the first prototype of T-GECO1, we fused calmodulin (CaM) and the CaM-binding
109 peptide (CBP) from ncpGCaMP6s to the mTFP1-derived fluorescent protein domain of
110 ZnGreen1.^{25,26} To further improve this prototype, we used multiple rounds of directed evolution.
111 In each round of directed evolution, we initially screened the fluorescence in the context of
112 *Escherichia coli* colonies, selecting for the brightest colonies for further testing. We then cultured
113 these variants and prepared clarified bacterial lysate using B-PER (Thermo Scientific). We
114 measured the fluorescence spectra in the absence of Ca²⁺ (EGTA, buffered in TBS, pH 7.3) and in

115 the presence of 10 nM and 10 mM Ca^{2+} (buffered in TBS, pH 7.3). The DNA encoding variants
116 with improved responses and high brightness was sequenced and used as the template for the next
117 round of library generation.

118 **2.2 Protein expression and purification**

119 The pBAD/HisB plasmid carrying the T-GECO1 gene was used to transform chemical or electro-
120 competent *E. coli* DH10B cells which were then grown on solid media. Single colonies were used
121 to inoculate a starter culture supplemented with ampicillin incubated at 37°C. After 4 hours, L-
122 arabinose was added to induce expression, and the culture was shaken overnight at 37°C before
123 harvesting the bacteria by centrifugation. The bacterial pellet was resuspended in 1× TBS, lysed
124 by sonication, and clarified by centrifugation. The cleared lysate was incubated with Ni-NTA
125 resin, washed, and eluted. Dialysis was done into 1× TBS using centrifugal filter units. All steps
126 were carried out at 4°C or on ice, unless specified otherwise.

127 **2.3 *In vitro* purified protein characterization**

128 To determine the apparent affinity for Ca^{2+} , buffers were prepared with varying concentrations of
129 free- Ca^{2+} ranging from zero to 39 μM by combining appropriate volumes of Ca^{2+} -free and Ca^{2+} -
130 containing stock solutions.²⁷ T-GECO1 was diluted in these buffered solutions, and the
131 fluorescence intensities of the protein in each solution was measured in triplicates. The obtained
132 measurements were plotted on a logarithmic scale against the concentration of free Ca^{2+} , and the
133 data was fitted to the Hill equation to determine the apparent K_d and apparent Hill coefficient.

134 To measure the extinction coefficient, the Strickler-Berg approach was used.²⁸ Briefly, purified
135 T-GECO1 protein was diluted in Ca^{2+} -free buffer (30 mM MOPS, 100 mM KCl, 10 mM EGTA,
136 pH 7.2), and Ca^{2+} containing buffer (30 mM MOPS, 100 mM KCl, 10 mM Ca-EGTA, pH 7.2).
137 The absorption, fluorescence emission, and excitation spectra for each sample were collected. For

138 fluorescence measurements, the samples were diluted to have optical densities less than 0.05.
139 Excitation spectra in both samples contain only the contribution from the anionic form of the
140 chromophore. Therefore, we calculated the integral of normalized absorption (entering the
141 Strickler-Berg equation) using corresponding excitation spectra. Fluorescence lifetimes and
142 quantum yields of the anionic chromophore were measured independently and then used in the
143 Strickler-Berg equation.

144 Fluorescence lifetimes were measured with a Digital Frequency Domain system ChronosDFD
145 appended to a PC1 spectrofluorimeter (both from ISS, Champaign, IL). Fluorescence was excited
146 with a 445-nm laser diode (ISS) through a 440/20 filter. The excitation was modulated with
147 multiple harmonics in the range of 10–300 MHz. Coumarin 6 in ethanol with $\tau = 2.5$ ns (ISS) was
148 used as a lifetime standard to obtain the instrumental response function in each measurement.
149 Fluorescence of the sample and standard were collected at 90° through a 520LP filter to cut off
150 scattered excitation light. The modulation ratio and phase delay curves were fitted to model
151 functions corresponding to a single- or double-exponential fluorescence decay with Vinci 3
152 software (ISS). Only double exponential decay functions provided acceptable χ^2 value of 0.5. The
153 main decay component, contributing ~93% of integrated decay in both samples was used in the
154 Strickler-Berg equation.

155 Fluorescence quantum yields were determined using the absolute method with an integrating
156 sphere instrument, Quantaaurus-QY (Hamamatsu). In this measurement, the quantum yield (QY)
157 was measured as a function of excitation wavelengths between 400 and 500 nm with the step of 5
158 nm. The quantum yield did not depend on wavelength in the region from 450 - 475 nm for the
159 Ca²⁺-bound state and from 465 – 480 nm for the Ca²⁺-free state, where the anionic absorption

160 dominated. The average of the quantum yields in these regions were calculated and presented in
161 the Results section. All measurements were made in triplicates and averaged.

162 **2.4 Two-photon measurements**

163 The two-photon excitation spectra and two-photon absorption cross-sections of T-GECO1 were
164 measured using a previously described protocol.²⁹ Briefly, a tunable femtosecond laser (InSight
165 DeepSee, Spectra-Physics, Santa Clara, CA) was coupled to a PC1 Spectrofluorometer (ISS,
166 Champaign, IL). Quadratic power dependence of fluorescence intensity was verified across the
167 spectrum for both proteins and standards. The two-photon cross-section (σ_2) of the anionic form
168 of the chromophore was determined for both the Ca^{2+} -free and Ca^{2+} -bound states, as previously
169 described.³⁰ As a reference standard, a solution of fluorescein in water at pH 12 was used.
170 Fluorescence intensities of the sample and reference were measured for two-photon excitation at
171 900 nm and for one-photon excitation at 458 nm (Ar^+ laser line). Fluorescence measurements
172 utilized a combination of filters (770SP and 520LP). The two-photon absorption spectra were
173 normalized based on the measured σ_2 values.

174 **2.5 Kinetic measurements**

175 Stopped flow kinetic measurements of Ca^{2+} binding and unbinding to T-GECO1 were made using
176 an Applied Photophysics SX20 Stopped-Flow Reaction Analyzer using fluorescence detection.
177 The deadtime of the instrument was 1.1 ms. The mixtures of the protein and Ca^{2+} (or EGTA, for
178 dissociation (or off) rate) were excited at 488 nm with 2 nm bandwidth and the emitted light was
179 collected at 515 nm through a 10-mm path. A total of 10,000 data points were collected over three
180 replicates ($n = 3$) at increments of 0.01 s for 5 seconds. For the off rate, T-GECO1 (diluted in 5
181 μM Ca^{2+} in TBS), was rapidly mixed 1:1 with 100 mM EGTA (diluted in TBS). Graphpad Prism
182 9 was used to fit the decrease in fluorescence intensity observed over time to a single exponential

183 dissociation. The k_{off} determined from this fit is the rate constant for dissociation of Ca^{2+} with units
184 of s^{-1} . For association (or on) rate, T-GECO1 was diluted in zero free CaEGTA buffer (Thermo
185 Scientific), and mixed 1:1 with varying Ca^{2+} concentrations (150 nM, 225 nM, 351 nM, 602 nM,
186 1.35 μM). The slope of k_{obs} vs. Ca^{2+} concentration was used to determine the k_{on} rate (with units
187 of $\text{s}^{-1}\text{M}^{-1}$).

188 **2.6 Neuronal stimulation**

189 T-GECO1, GCaMP6s, and jGCaMP8s, were cloned and packaged into AAV2/1 virus under
190 control of the hSyn promoter. The AAVs were used to transduce hippocampal and cortical mixture
191 primary cultures from neonatal (P0) pups in poly-D-lysine-coated 24-well glass bottom plates.
192 After 14 days post transduction, the culture medium was exchanged with 1 mL imaging buffer
193 (145 mM NaCl, 2.5 mM KCl, 10 mM glucose, 10 mM 4-(2-hydroxyethyl)piperazine-1-
194 ethanesulfonic acid (HEPES), 2 mM CaCl_2 , 1 mM MgCl_2 , pH 7.3) containing 10 μM 6-cyano-7-
195 nitroquinoxaline-2,3-dione (CNQX), 10 μM 3-((*R*)-2-carboxypiperazin-4-yl)-propyl-1-
196 phosphonic acid ((*R*)-CPP), 10 μM gabazine, and 1 mM (*S*)- α -methyl-4-carboxyphenylglycine
197 ((*S*)-MCPG) (Tocris). Neurons were field stimulated with 1, 3, 10, and 20 pulses at 30 Hz, and
198 imaged through a 20 \times objective, with excitation at 470/40 nm. Imaging was performed at room
199 temperature.

200 **2.7 Preparation of organotypic hippocampal slice cultures for two-photon Ca^{2+}** 201 **imaging using T-GECO1 and jGCaMP7s**

202 Organotypic hippocampal slices were prepared from postnatal day 8 (P8) mice (Janvier Labs,
203 C57Bl/6J). Hippocampi were dissected and sectioned into 300 μm thick slices using a tissue
204 Chopper (McIlwain type 10180, Ted Pella), in a cold dissection medium consisting of GBSS
205 (Sigma, G9779) that was supplemented with 25 mM D-glucose, 10 mM HEPES, 1 mM Na-

206 pyruvate, 0.5 mM α -tocopherol, 20 nM ascorbic acid, and 0.4% penicillin/streptomycin (5000 U
207 mL⁻¹).

208 Slices were incubated for 45 minutes at 4 °C in the dissection medium, then placed on a porous
209 membrane (Millipore, Millicell CM PICM03050) and cultured at 37 °C, 5% CO₂ in a medium
210 consisting of 50% Opti-MEM (Fisher 15392402), 25% heat-inactivated horse serum (Fisher
211 10368902), 24% HBSS, 1% penicillin/streptomycin (5000 U mL⁻¹), and supplemented with 25
212 mM D-glucose, 10 mM HEPES, 1 mM Na-Pyruvate, 0.5 mM α -tocopherol, 20 nM ascorbic acid,
213 and 0.4% penicillin/streptomycin (5000 U mL⁻¹). After three days *in vitro* (DIV), this medium was
214 replaced with one consisting of 82% neurobasal-A (Fisher 11570426), 15% heat-inactivated horse
215 serum (Fisher 10368902), 2% B27 supplement (Fisher, 11530536), 1% penicillin/streptomycin
216 (5000 U mL⁻¹), 0.8 mM L-glutamine, 0.8 mM Na-Pyruvate, 10 nM ascorbic acid and 0.5 mM α -
217 tocopherol. This medium was removed and replaced every 2-3 days. Slices were transduced with
218 AAVs at DIV 3 by bulk application of 1 μ L of virus per slice, for expression of T-GECO1 or
219 jGCaMP7s under control of the hSyn promoter. Experiments were performed at DIV 10.

220 **2.8 Two-photon Ca²⁺ imaging of action potentials in T-GECO1- and jGCaMP7s-** 221 **expressing organotypic hippocampal slices**

222 At DIV 10, whole-cell current clamp recordings of T-GECO1- or jGCaMP7s-expressing neurons
223 were performed at room temperature (21 - 23°C). A commercial upright microscope (Zeiss, Axio
224 Examiner.Z1), equipped with a microscope objective (Zeiss, W Plan-Apochromat 20X, 1.0 NA)
225 and an sCMOS camera (Photometrics, Kinetix), was used to collect light transmitted through the
226 sample. Patch-clamp recordings were performed using an amplifier (Molecular Devices,
227 Multiclamp 700B) and a digitizer (Molecular Devices, Digidata 1440A), at a sampling rate of 10
228 kHz using pCLAMP10 (Molecular Devices). During the experiments, slices were continuously

229 perfused with artificial cerebrospinal fluid (ACSF) composed of 125 mM NaCl, 2.5 mM KCl, 1.5
230 mM CaCl₂, 1 mM MgCl₂, 26 mM NaHCO₃, 0.3 mM ascorbic acid, 25 mM D-glucose, 1.25 mM
231 NaH₂PO₄. ACSF was supplemented with 1 μM AP5 (Abcam, ab120003), 1 μM NBQX (Abcam,
232 ab120046), and 10 μM picrotoxin (Abcam, 120315). Continuous aeration of the recording solution
233 with 95% O₂ and 5% CO₂ resulted in a pH of 7.4. Patch pipettes were pulled from borosilicate
234 glass capillaries (with filament, OD: 1.5 mm, ID: 0.86 mm, 10 cm length, fire polished, WPI) using
235 a Sutter Instruments P1000 puller, to a tip resistance of 4.5 – 5.5 MΩ, and filled with an
236 intracellular solution consisting of 135 mM K-gluconate, 4 mM KCl, 4 mM Mg-ATP, 0.3 mM
237 Na₂-GTP, 10 mM Na₂-phosphocreatine, and 10 mM HEPES (pH 7.35). Only recordings with an
238 access resistance below 20 MΩ were included in subsequent analysis. In the current-clamp
239 configuration, the bridge potential was corrected (bridge potential = 13.9 ± 1.0 MΩ; mean ± s.d.).

240 Two-photon scanning imaging was performed with a Ti:sapphire tunable pulsed laser (Spectra
241 Physics, Mai-Tai DeepSee, pulse width ≈ 100 fs, repetition rate 80 MHz, tuning range 690 – 1040
242 nm), going through a commercial galvo-galvo scanning head (3i, Vivo 2-photon) operated using
243 Slidebook 6 software. The detection axis consisted of a PMT with a 510/84 nm bandpass filter
244 (Semrock, FF01-510/84). Imaging was performed within a 365 × 365 μm field of view (FOV) at
245 a rate of 3.05 Hz (bidirectional scanning, 256 × 256 pixels, pixel size 1.4 μm, dwell time 4.0 μs).
246 Laser power was controlled by a Pockels cell (Conoptics, 350-80). Prior to the experiments,
247 powers were measured at the output of the objective using a thermal sensor power meter (Thorlabs,
248 PM100D).

249 Action potentials were triggered by injecting current for 5 ms (ranging from 500 to 1200 pA),
250 at a rate of 30 Hz during a period ranging from 5 ms to 650 ms, in order to evoke the desired

251 number of action potentials, while the FOV was scanned under 850 nm or 920 nm illumination at
252 20 mW. Recordings were dismissed if the desired amount of action potentials failed to occur.

253 Fluorescence intensities were integrated over regions of interest (ROI) covering the patched
254 neuron soma. Percentage changes in fluorescence were calculated as $\Delta F/F_0 = (F - F_0)/F_0$, where
255 F_0 is the basal level of fluorescence measured, averaged over 35 frames (≈ 12 s) before the
256 triggering of action potentials. SNR was measured as $SNR = F/\sigma_{F0}$, where σ_{F0} represents the
257 standard deviation of the fluorescence F over the 35 frames prior to the stimulation.

258 **2.9 Evaluation of crosstalk induced by the two-photon scanning laser in ChromE-** 259 **expressing organotypic hippocampal slices**

260 At DIV 3, organotypic hippocampal slices were infected with a mixture of
261 AAV9.hSyn.DIO.ChroME.Flag.ST.P2A.H2B.mRuby3.WPRE.SV40 (titer = $5.9E12$ GC mL⁻¹)
262 and AAV9.hSyn.Cre.WPRE.hGH (titer = $2.3E11$ GC mL⁻¹) by bulk application of 1 μ L of the
263 mixture.

264 At DIV 10, whole-cell current clamp recordings of ChromE-expressing cells were performed
265 in the same conditions as described above. The membrane potential of the patched neuron was
266 monitored and recorded while scanning the FOV for 30 s ($365 \times 365 \mu\text{m}^2$, 256×256 pixels, pixel
267 size 1.4 μm) at 850 nm or 920 nm, at 20 mW, and at acquisition rates of 1.5 Hz, 3.05 Hz and 6 Hz
268 (corresponding to dwell time per pixel of 6 μs , 4 μs and 2 μs respectively). The variation of
269 membrane potential ΔV_m reported in the manuscript corresponds to the average of the amplitude
270 of the depolarization peaks induced by the imaging laser, during a 30 s scanning epoch.
271 Depolarization peaks were measured as $\Delta V_m = V_{mp} - V_{m0}$, where V_{mp} is the peak of the membrane
272 potential depolarization (one for each frame) and V_{m0} is the membrane potential of the neuron

273 measured just before the beginning of the scanning. The ratio $\Delta V_{m850}/\Delta V_{m920}$, was calculated for
274 each cell, and then averaged across cells.

275 **2.10 Stereotaxic injection and fiber implant surgery**

276 Stereotaxic injections of AAVs and optical fiber implant surgeries were performed at the same
277 time in C57BL/6J mice (The Jackson Laboratory, #000664) at around P60. Mice were anesthetized
278 with isoflurane and monitored throughout the surgery with tail pinch and breathing rate. First, the
279 skin above the skull was cleaned and removed to allow attachment of the headframe and optical
280 fiber implants. Next, a burr hole craniotomy was drilled above the fiber implant coordinates for
281 implantation in the nucleus accumbens core (AP: 1.2 mm, ML: 1.3 mm, DV: 4.1 mm). Virus
282 injection of either AAV2/1-hSyn-T-GECO1 (100 nL, titer = $1.5E13$ GC mL⁻¹) or AAV2/1-hSyn-
283 jGCaMP8s (100 nL, titer = $1.9E13$ GC mL⁻¹) was performed with a glass pipette prior to fiber
284 implant. Following virus injection, a fiber optic probe was positioned above the same coordinates
285 and the tip of the fiber was lowered to 100 μ m above the virus injection. The fiber implant was
286 then affixed to the skull with dental cement. A custom headframe was then positioned on the skull
287 and glued in place with dental cement to allow head-fixation during photometry. The mice were
288 allowed to recover for two weeks before the start of imaging. All photometry was performed in
289 head-fixed mice placed on a running wheel to allow spontaneous running.

290 **2.11 Fiber photometry measurement and analysis**

291 Fiber photometry measurements were performed on a custom spectral photometry system. 448 nm
292 (Coherent, OBIS 445 nm LX 365 mW LASER, measured wavelength is 448 nm) and 473 nm
293 (Coherent, OBIS 473 nm LX 200 mW LASER, measured wavelength is 473 nm) excitation lasers
294 were co-aligned and focused onto the back pupil of an objective (Nikon, Plan Apochromat, 10X,
295 0.45 NA, 25 mm FOV). The excitation light was coupled into a fiber optic patch cable (Doric, 200

296 μm core, 0.37 NA) by positioning the patch cable at the image plane of the objective. The other
297 end of the patch cable was coupled to the implanted fiber stub. Emitted light from the brain tissue
298 was collected through the same fiber probes and patch cable and passed through a polychromator
299 (Edmund Optics, 50 mm N-SF11 equilateral prism). The polychromator spreads the image of the
300 fiber tip according to its spectrum, which was imaged onto a sCMOS camera sensor (Hamamatsu,
301 Orca Flash 4.0 v3). The excitation lasers and camera sensor were triggered synchronously using
302 an Arduino Teensy board (the excitation lasers were sequentially triggered while the camera sensor
303 was triggered at every frame) at 24 Hz frame rate. The raw images were acquired and saved
304 through a custom script in the Bonsai reactive programming environment.³¹ The recorded spectra
305 corresponding to either T-GECO1 (485-510 nm) or jRCaMP8s (520-545 nm) emission were
306 averaged to yield a single intensity time trace. The fractional intensity change was computed by
307 dividing the intensity of each frame by the mean fluorescence of the full trace over time.

308 **2.12 Animal care**

309 Animal experiments at Sorbonne Université were conducted in accordance with guidelines from
310 the European Union and institutional guidelines on the care and use of laboratory animals (Council
311 Directive 2010/63/EU of the European Union). Surgery protocol and fiber photometry imaging
312 experiments at the Allen Institute for Neural Dynamics were approved by the Allen Institute
313 Institutional Animal Care and Use Committee (IACUC). Animal experiments at Janelia Research
314 Campus were conducted according to National Institutes of Health guidelines for animal research
315 and were approved by the Janelia Research Campus Institutional Animal Care and Use Committee
316 and Institutional Biosafety Committee. Procedures in the United States conform to the National
317 Institutes of Health (NIH) Guide for the Care and Use of Laboratory Animals. Mice were housed

318 under controlled temperature (approximately 21 °C) and humidity (approximately 50%) conditions
319 under a reverse light cycle.

320 **3 Results**

321 **3.1 Development of mTFP1-based genetically encoded Ca²⁺ indicator, T-GECO1**

322 Our initial template for constructing an mTFP1-based GEI was the mTFP1-based genetically
323 encoded Zn²⁺ indicator, ZnGreen1.²⁵ ZnGreen1 consists of the Zap1 zinc finger inserted into a
324 further engineered version of mTFP1. This version of mTFP1 in ZnGreen1 harbors the nine
325 additional mutations N42H, N81D, D116G, S146C, T147D, R149K, E168K, R198H, V218A
326 using mTFP1 numbering (or N42H, N81D, D116G, S323C, T324D, R326K, E345K, R375H,
327 V395A using T-GECO numbering). To construct the initial prototype mTFP1-based GEI,
328 designated T-GECO0.1, we replaced the Zap1 zinc finger of ZnGreen1 with the fused calmodulin
329 (CaM) and CaM-binding peptide (CBP) domain from ncpGCaMP6s.²⁶ The linker sequences from
330 ZnGreen1 were retained. The arrangement of these domains is represented in **Fig. 1a**.

331 As previously described, we define the linkers as additional residues that are inserted between
332 the Ca²⁺-binding domain (CaM fused to CBP) and the gatepost residues 143 and 146 of mTFP1.³²
333 In T-GECO0.1 the linker from the first mTFP1 gatepost (W143) to CaM linker (Linker 1) is Leu-
334 Gly-Asn. Linker 2 from CBP to the second mTFP1 gatepost (S146C) is a single Pro. To develop
335 further improved T-GECO variants, we first optimized these linker residues and some adjacent
336 positions. This was achieved by randomizing each residue, expressing the resulting library in *E.*
337 *coli*, picking and culturing bright colonies, and testing Ca²⁺-dependent responses in bacterial
338 lysates. Ultimately, we identified Arg-Asn-Arg as the optimal Linker 1, and Ile as the optimal
339 Linker 2 (**Fig. 1a**).

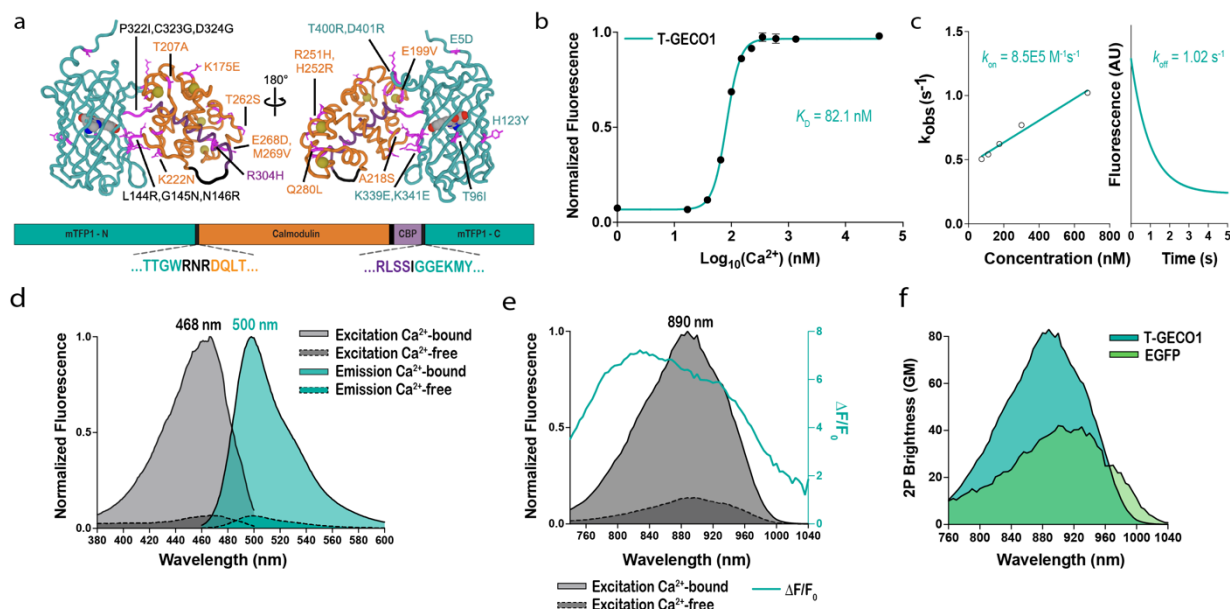
340 Further optimization by directed evolution was performed by generating libraries using
341 error-prone (EP) PCR amplification of the entire coding sequence of T-GECO. In each round, we
342 took variants with moderate to high fluorescence change upon binding Ca^{2+} and measured their
343 affinity, pH response, quantum yield, and extinction coefficient. We obtained the DNA sequence
344 of these variants and used them as the template for the next round of iterative directed evolution.
345 Following five generations of screening, we arrived at T-GECO1 on the basis of its high $\Delta F/F_0$,
346 high affinity, high brightness, two-photon cross-section, and kinetics. T-GECO1 has 25 mutations
347 with respect to T-GECO0.1 (E5D, T96I, H123Y, L144R, G145N, N146R, K175E, E199V, T207A,
348 A218S, K222N, R251H, H252R, T262S, E268D, M269V, Q280L, R304H, P322I, C323G,
349 D324G, K339E, K341E, T400R, D401R, using T-GECO numbering). There are 4 mutations in
350 the linkers, 9 mutations in the mTFP1-derived region, 11 mutations in CaM, and 1 mutation in
351 CBP. The locations of all mutations are shown in **Fig. 1a** and **Fig. 2**.

352 We first characterized the photophysical properties of T-GECO1 as a soluble protein under
353 one-photon and two-photon excitation (**Fig. 1b-f**). Under one-photon excitation, T-GECO1 in the
354 Ca^{2+} -bound state exhibits excitation and emission peaks at 468 nm and 500 nm, respectively. The
355 molecular brightness of T-GECO1 in the Ca^{2+} -bound state, calculated as the product of the
356 extinction coefficient ($49,300 \text{ M}^{-1}\text{cm}^{-1}$) and quantum yield (0.83), is similar to that of EGFP (**Table**
357 **1**).¹⁷ The two-photon excitation maximum of T-GECO1 is 888 nm with a brightness of 83 GM,
358 which is 1.4× the value of mTFP1 and 2× the value of EGFP (**Table 2**). T-GECO1 exhibits a large
359 change in fluorescence intensity upon addition of Ca^{2+} , with 1-photon peak $\Delta F/F_0$ of 15 and 2-
360 photon peak $\Delta F/F_0$ of 7, where $\Delta F/F_0 = (F_{\text{max}} - F_{\text{min}})/F_{\text{min}}$. Additionally, we determined that T-
361 GECO1 has an apparent K_d of 82 nM for binding to Ca^{2+} , and an apparent Hill coefficient (n_H) of

362 3.6. T-GECO1 exhibits moderate binding (on) and dissociation (off) kinetics as soluble protein,
363 with k_{on} of $8.5 \times 10^5 \text{ M}^{-1}\text{s}^{-1}$ and k_{off} of 1.02 s^{-1} .

364 Together, these results demonstrate T-GECO1 has favorable photophysical characteristics
365 that make it a potentially useful new GECI. Its high fluorescence change upon binding Ca^{2+} , high
366 brightness and two-photon cross-section, and reasonable association and dissociation kinetics
367 suggest that T-GECO1 is a promising tool for monitoring Ca^{2+} dynamics using blue-shifted
368 excitation.

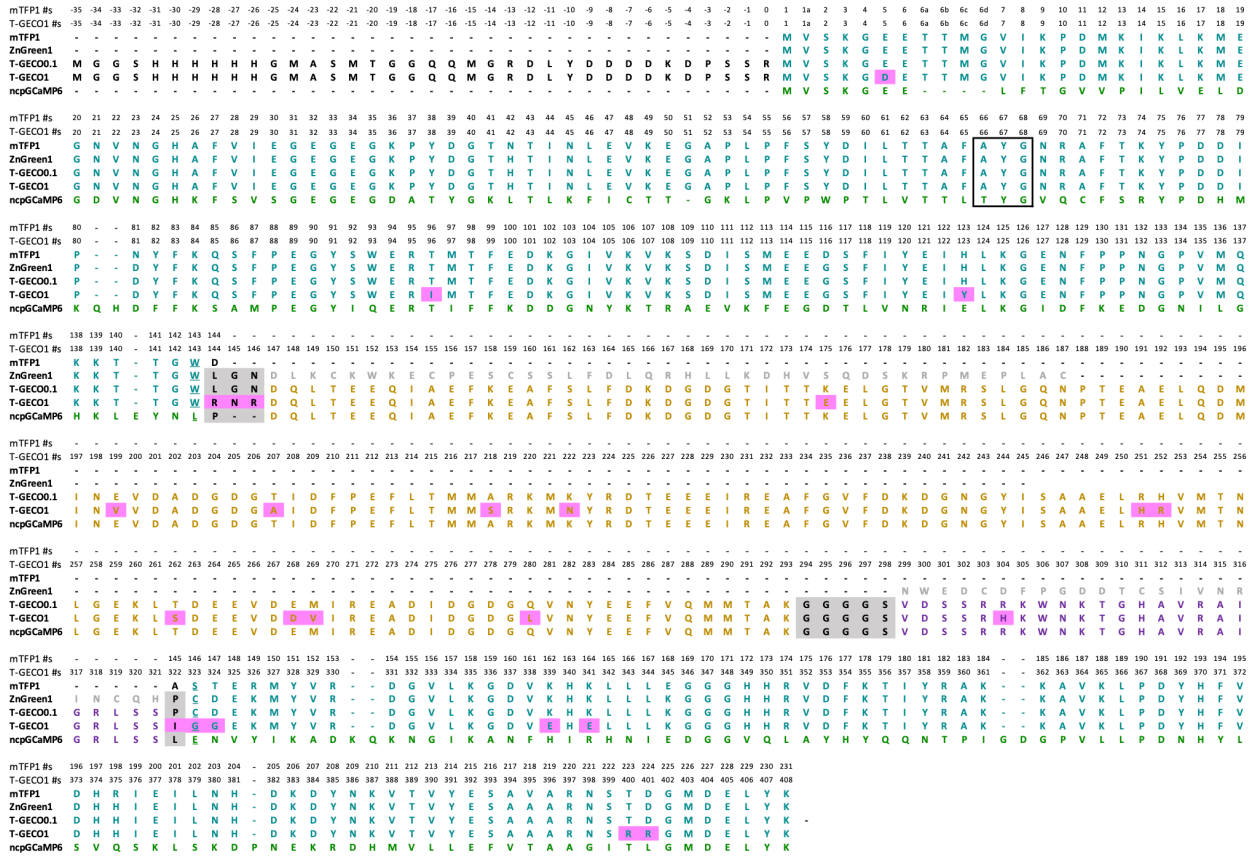
369



370

371 **Fig. 1.** Development and characterization of T-GECO1 as a purified protein. (a) Two views of the
372 modeled structure of the Ca²⁺-bound state of T-GECO1. For the structure representation, mutated
373 residues are shown as magenta sticks, Ca²⁺ is shown as yellow spheres, and the chromophore
374 is shown in space-filling representation. Both the protein structure and the labels are shown in
375 teal for the mTFP1-derived domain, in orange for the CaM domain, in purple for the CaM-binding
376 peptide, and in black for linkers. Colors are consistent with the sequence alignment shown as **Fig.**
377 **2.** The overall structure was predicted using ColabFold.³³ The chromophore was positioned using
378 PyMol (Version 2.5.4 Schrödinger, LLC.) to superimpose the structure of mTFP1 (PDB ID
379 2HQK)²³ with the fluorescent protein portion of the T-GECO1 model. Ca²⁺ ions were similarly
380 positioned by superimposing the CaM domain of GCaMP2 (PDB ID 3EVR)³⁴ with the CaM portion
381 of the T-GECO1 model. (b) Ca²⁺ titration of T-GECO1. (c) Stopped-flow kinetic measurements of
382 the fluorescence response of T-GECO1 for Ca²⁺ association (left) and dissociation (right). (d)
383 Excitation and emission spectra of T-GECO1 in the presence and absence of Ca²⁺. (e) Two-
384 photon excitation-induced fluorescence of T-GECO1 as a function of wavelength, in the presence

385 and absence of Ca^{2+} , with $\Delta F/F_0$ represented in teal. (f) Two-photon cross-section of T-GECO1
386 in the Ca^{2+} -bound state, compared to the two-photon cross-section of EGFP.
387



388

389

Fig. 2. Sequence alignment of T-GECO1 and related proteins. Residues are colored teal for the

390

mTFP1-derived domain, orange for the CaM domain, purple for the CaM-binding peptide, and

391

black on a gray background for the linkers. Mutated residues are shown on a magenta

392

background. A black box encloses the chromophore-forming tripeptide. The gatepost residues

393

143 and 146 (using mTFP1 numbering) are underlined.³² Colors are consistent with the structural

394

model shown in **Fig. 1a**.

395 **Table 1.** One-photon photophysical properties of T-GECO1 and mTFP1,²⁸ measured as purified
 396 proteins ($n = 3$, averaged). Extinction coefficients were obtained using Strickler-Berg formula.²⁸ In
 397 this calculation, the main fluorescence lifetime component of T-GECO1 was used. Note that the
 398 relative values of the brightness of the Ca^{2+} -bound and Ca^{2+} -free fluorescent states shown here
 399 do not represent the Ca^{2+} -dependent fluorescence change of T-GECO1. The Ca^{2+} -dependent
 400 fluorescence change is primarily due to a change in the protonation state of the chromophore
 401 which changes the fraction of the protein in fluorescent state.

Property	T-GECO1 Ca^{2+} -bound	T-GECO1 Ca^{2+} -free	mTFP1 (ref. ²⁸)	EGFP (ref. ¹⁷)
Absorption maxima λ_{ex} (nm)	468	470	463	489
Emission maxima λ_{em} (nm)	500	502	494	510
Ca^{2+} -dependent $\Delta F/F_0$	15		n/a	n/a
K_d (nM)	82		n/a	n/a
Apparent Hill coefficient (n_H)	3.6		n/a	n/a
Fluorescence lifetime τ (ns)	3.1 (93%); 1.5 (7%) < τ > = 2.95 (integral)	3.1 (92%); 1.2 (8%) < τ > = 2.96 (integral)	3.2	2.7
Extinction Coefficient ($\text{M}^{-1}\text{cm}^{-1}$)	49,300	43,000	48,000	58,300
Quantum Yield	0.83	0.76	0.84	0.76
Brightness ($\text{EC} \times \text{QY}$, $\text{mM}^{-1} \text{cm}^{-1}$)	40.9	32.7	40.3	44.3

402

403 **Table 2.** Two-photon photophysical properties of T-GECO1 (Ca²⁺-bound state), mTFP1, and
404 EGFP, measured as purified proteins (n = 3, averaged). Values for mTFP1 and EGFP have were
405 previously reported.^{17,28}

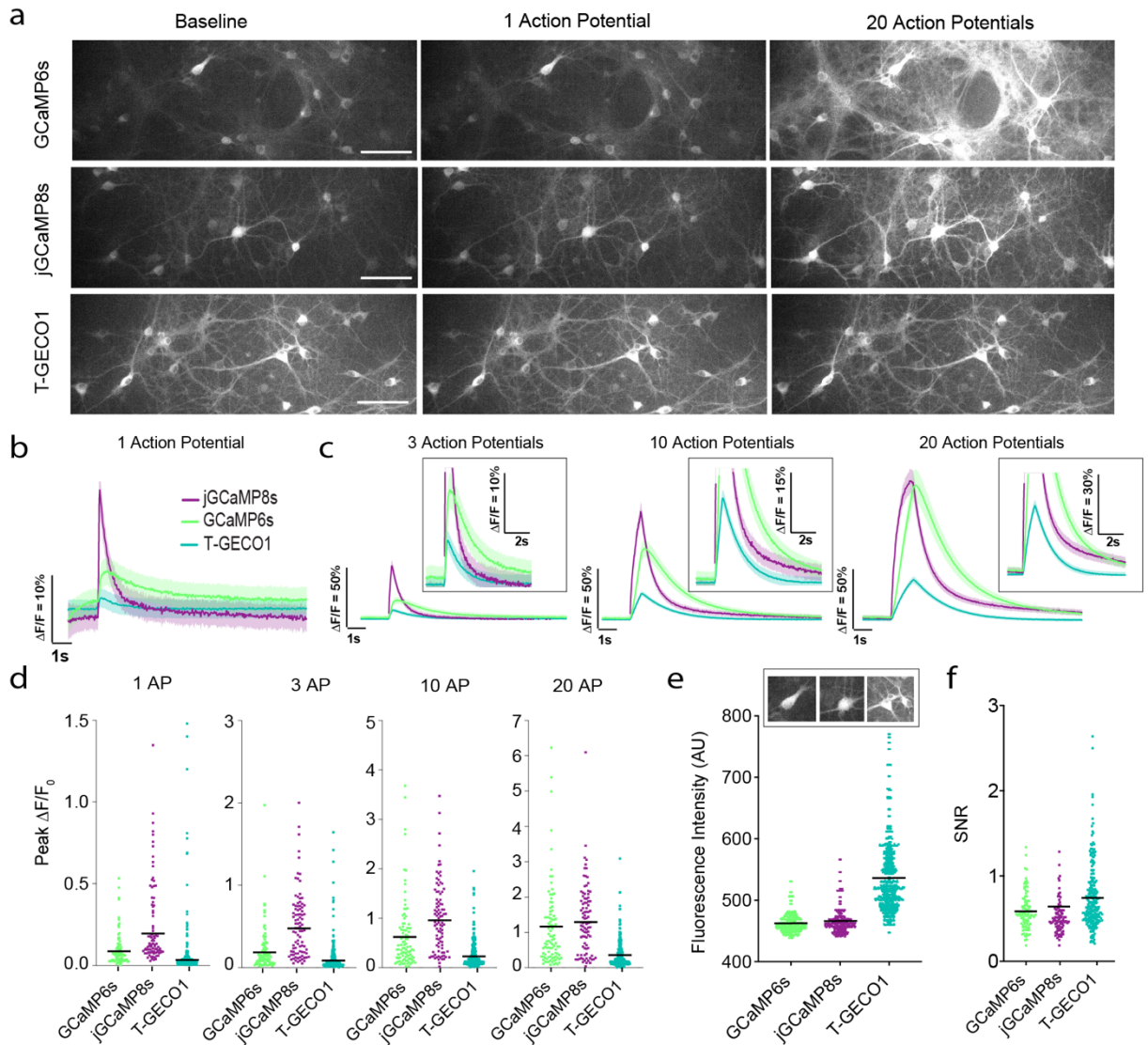
Property	T-GECO1	T-GECO1	mTFP1	EGFP
	Ca ²⁺ -bound	Ca ²⁺ -free		
Two-photon cross-sections (GM) with λ_{\max} in parentheses	100 (888 nm)	82 (896)	70 (875 nm)	54 (911 nm)
Two-photon brightness F_2 (GM) with λ_{\max} in parentheses	83 (888 nm)	62 (896)	60 (875 nm)	41 (911 nm)
Two-photon $\Delta F/F_0$	7.4		n/a	n/a

406

407 **3.2 Imaging of Ca²⁺ in electric field stimulated neuronal cultures**

408 To characterize T-GECO1 in neuronal cultures using one-photon excitation (excitation at 450 -
409 490 nm), we expressed it under the control of human synaptic (hSyn) promoter in rat primary
410 cortical and hippocampal neurons. We compared the performance of T-GECO1 to GCaMP6s and
411 jGCaMP8s (**Fig. 3a**). To evoke neuronal activity, we applied trains of 1, 3, 10, and 20 electric field
412 stimuli and analyzed the resulting fluorescence changes (**Fig. 3b,c,d**). T-GECO1 exhibited a peak
413 change in fluorescence ($\Delta F/F_0$) of 3% for a single stimulus. In comparison, GCaMP6s and
414 jGCaMP8s had peak responses of 9% and 20%, respectively, in response to single stimuli. T-
415 GECO1 exhibited lower $\Delta F/F_0$ values across all numbers of stimuli tested. The baseline brightness
416 of T-GECO1 (536 +/- 59 RFU), was found to be 16% higher than that of GCaMP6s (463 +/- 16
417 RFU) and 15% higher than that of jGCaMP8s (466 +/- 21 RFU) (**Fig. 3e**). T-GECO1 exhibited a
418 marginally larger SNR compared to GCaMP6s and jGCaMP8s, partially due to its higher baseline
419 brightness (**Fig. 3f**).

420 These results demonstrate that T-GECO1 has sufficient sensitivity for detecting small
421 numbers of action potentials in cultures, using one-photon excitation. However, further
422 optimization will be necessary to achieve the peak sensitivity exhibited by late-generation GCaMP
423 series indicators. Nevertheless, T-GECO1's higher baseline brightness and blue-shifted excitation
424 and emission may prove advantageous, relative to the GCaMP series, for certain one-photon
425 excitation applications such as multicolor imaging and combined use with longer-wavelength
426 activatable optogenetic tools.



427

428 **Fig. 3.** Characterization of T-GECO1 in rat cultured neurons. (a) Images of primary rat
 429 hippocampal cultured neurons expressing GCaMP6s, jGCaMP8s, and T-GECO1 under the hSyn
 430 promoter at baseline, and after field stimulations of 1 and 20 action potentials (APs) at room
 431 temperature. (b) Normalized $\Delta F/F_0$ traces for stimulations at 1 AP and (c) 3 AP, 10 AP, and 20
 432 AP at 30 Hz. (d) Peak $\Delta F/F_0$ of the three sensors across the same conditions. (e) Baseline
 433 brightness of the three sensors. (f) Signal-to-noise ratio (SNR) for the three variants across
 434 conditions. Traces and error bars denote mean \pm s.e.m. Each data point is one ROI and is
 435 pooled across three independent wells.

436 **3.3 Two-photon Ca²⁺ imaging of T-GECO1 in organotypic hippocampal slices.**

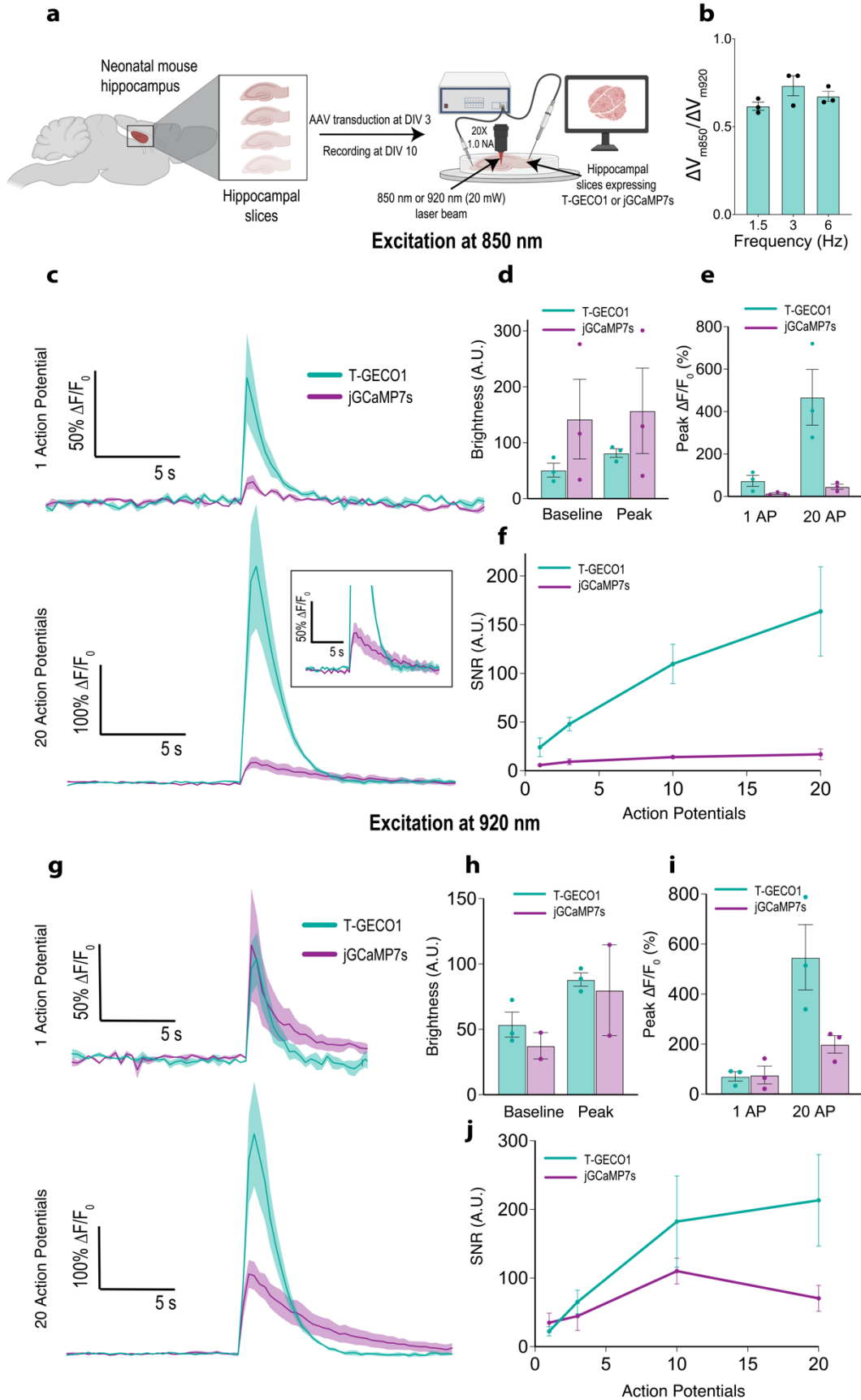
437 Next, we compared the performance of T-GECO1 to jGCaMP7s (ref. ³) using two-photon Ca²⁺
438 imaging in neonatal mouse organotypic hippocampal slices (**Fig. 4a**). We hypothesized that, due
439 to its blue-shifted two-photon excitation maxima relative to GCaMP7s's (**Fig. 1f**), T-GECO1
440 could be the more suitable choice for all-optical stimulation and imaging when used in conjunction
441 with the ChroME opsin.³⁵ Specifically, we expected that excitation wavelengths that are near-
442 optimal for T-GECO1 (i.e., ~850 nm) would result in less undesirable activation of ChroME than
443 excitation wavelengths that are near-optimal for GCaMP7s (i.e., ~920 nm). To test this hypothesis,
444 we quantified the change in membrane potential when ChroME-expressing neurons were
445 illuminated with either 850 nm or 920 nm and expressed the ratio calculated as $\Delta V_{m850}/\Delta V_{m920}$, on
446 a cell-by-cell basis. Across all tested frequencies (1.5, 3, and 6 Hz), this ratio consistently remained
447 below one (0.62, 0.73, 0.67), indicating that using an imaging wavelength of 850 nm rather than
448 920 nm is advantageous for reducing undesirable ChroME activation (**Fig. 4b**).

449 We next investigated the fluorescence responses of both T-GECO1 and GCaMP7s at excitation
450 wavelengths of 850 nm and 920 nm, with varying numbers of stimulated action potentials (APs)
451 (**Fig. 4a**). Under excitation at 850 nm, T-GECO1 exhibited a fluorescence change ($\Delta F/F_0$) of 73%,
452 whereas jGCaMP7s exhibited a change of 13%, in response to 1 AP (**Fig. 4c,e**). In response to 20
453 APs, T-GECO1 exhibited a fluorescence change of 450% and jGCaMP7s exhibited a change of
454 38% (**Fig. 4c,e**). The signal-to-noise ratio (SNR) for T-GECO1 was substantially higher than for
455 jGCaMP7s (**Fig. 4f**).

456 When excited at 920 nm, the differences between the two indicators were marginal. At 1 AP,
457 both T-GECO1 and jGCaMP7s displayed similar $\Delta F/F_0$ values (65% and 75%, respectively). For
458 20 APs, T-GECO1 exhibited a $\Delta F/F_0$ of 547%, approximately 2.8 times greater than the $\Delta F/F_0$ of

459 jGCaMP7s (194%) (**Fig. 4g, i**). The baseline brightness of T-GECO1 before stimulation was
460 higher than that of jGCaMP7s (53.6 AU for T-GECO1 and 37.5 AU for jGCaMP7s) and remained
461 higher at its peak after stimulation (88.1 AU and 79.9 AU, respectively) (**Fig. 4h**). Similar to the
462 850 nm excitation, the SNR of T-GECO1 was consistently higher than that of jGCaMP7s (**Fig.**
463 **4j**).

464 These results indicate that T-GECO1 may offer substantial performance advantages relative to
465 jGCaMP7s under two-photon excitation conditions, particularly at the excitation wavelength of
466 850 nm. This apparent advantage is consistent with our original rationale for using mTFP1, which
467 is itself particularly bright under two-photon excitation, as the starting point for developing a new
468 Ca²⁺ indicator.



470 **Fig. 4.** Two-photon Ca^{2+} imaging of T-GECO1 in organotypic hippocampal slices. **(a)** Schematic
471 of the setup. **(b)** $\Delta V_{m850}/\Delta V_{m920}$ ratio of ChroME-expressing organotypic hippocampal slices. **(c)**
472 Representative traces of T-GECO1 (teal) and jRCaMP7s (purple) for 1 action potential (top) and
473 20 action potentials (bottom) excited at 850 nm. **(d)** Baseline brightness (A.U) for the two
474 indicators at baseline (before stimulation) and at peak (maximum brightness after stimulation) at
475 850 nm excitation. **(e)** Peak $\Delta F/F_0$ (%) for the two indicators at 1 or 20 action potentials at 850 nm
476 excitation. **(f)** SNR (signal-to-noise ratio) for the two indicators with respect to action potentials at
477 850 nm excitation. **(g)** Representative traces of T-GECO1 (teal) and jRCaMP7s (purple) for 1
478 action potential (top) and 20 action potentials (bottom) excited at 920 nm. **(h)** Baseline brightness
479 (A.U) for the two indicators at baseline (before stimulation) and at peak (maximum brightness
480 after stimulation) at 920 nm excitation. **(i)** Peak $\Delta F/F_0$ (%) for the two indicators at 1 or 20 action
481 potentials at 920 nm excitation. **(j)** SNR (signal-to-noise ratio) for the two indicators with respect
482 to action potentials at 920 nm excitation. Error bars denote +/- S.E.M.

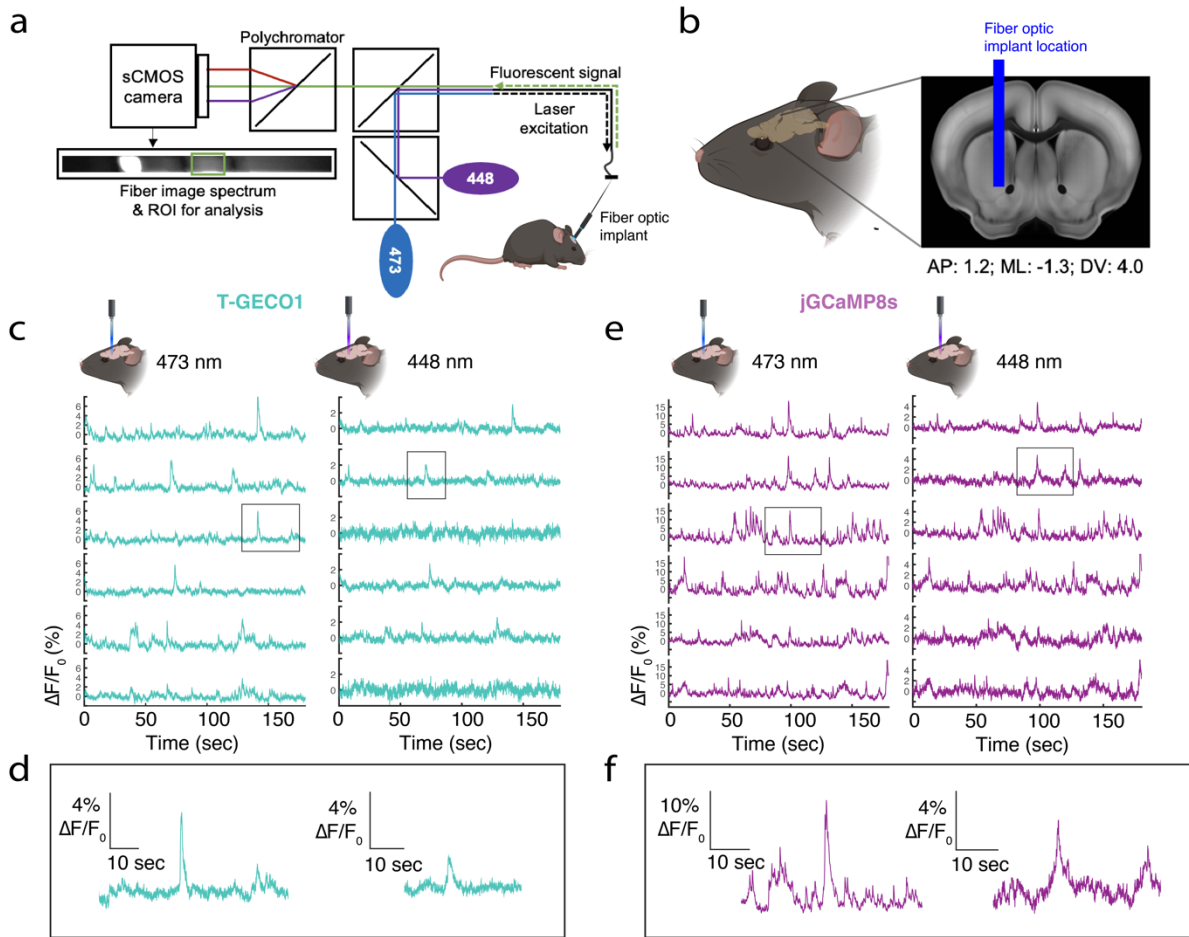
483 **3.4 *In vivo* Ca²⁺ detection in the nucleus accumbens using fiber photometry**

484 To evaluate the performance of T-GECO1 in the intact brain using one-photon excitation, we
485 conducted fiber photometry measurements by expressing either T-GECO1 or jGCaMP8s in the
486 nucleus accumbens of mice. Fluorescence traces were recorded using fiber implants positioned
487 above the injection site (**Fig. 5a,b**). We excited both T-GECO1 and jGCaMP8s using either 448
488 nm or 473 nm wavelengths while the mice engaged in spontaneous running, with occasional
489 manual whisker flicking to evoke Ca²⁺ transients. T-GECO1 enabled reliable detection of Ca²⁺
490 transients at both 473 nm and 448 nm excitation wavelengths, with higher fluorescence changes
491 ($\Delta F/F_0$) observed at 473 nm compared to 448 nm (**Fig. 5c,d**). In general, these responses were
492 substantially lower than those observed with jGCaMP8s, regardless of the excitation wavelength
493 used (**Fig. 5e,f**).

494 These *in vivo* imaging results are qualitatively consistent with the results from *in vitro*
495 imaging in neuronal cultures, using one-photon excitation. That is, T-GECO1 can be effectively
496 utilized for *in vivo* one-photon excitation imaging of neuronal activity using either 448 nm or 473
497 nm excitation, but does not achieve the peak sensitivity exhibited by late-generation GCaMP series
498 indicators.

499

500



501

502 **Fig. 5.** *In vivo* Ca²⁺ detection in the nucleus accumbens using fiber photometry. (a) Simplified
503 schematic illustrating the fiber photometry setup, featuring two excitation wavelengths of 473 nm
504 and 448 nm. (b) Precise position of the fiber optic implant. (c) Representative fluorescence traces
505 of T-GECO1 at 473 nm excitation (left) and 448 nm excitation (right). (d) Zoomed-in view of the
506 outlined traces displayed in (c). (e) Representative fluorescence traces of jRCaMP1s at 473 nm
507 excitation (left) and 448 nm excitation (right). (f) Zoomed-in view of the outlined traces displayed
508 in (e).

509 **4 Discussion**

510 To expand the GECI color palette we developed a novel Ca^{2+} indicator, T-GECO1, based on
511 mTFP1. In this manuscript, we have reported the development and characterization of T-GECO1,
512 and compared it against state-of-the-art GCaMP series indicators for imaging of neuronal activity.
513 We performed this comparison in three different contexts: *in vitro* one-photon excitation in
514 cultured rat hippocampal neurons, *in vivo* one-photon excitation fiber photometry in mice, and *ex*
515 *vivo* two-photon Ca^{2+} imaging in hippocampal slices.

516 As we had hoped when we embarked on the development of this new Ca^{2+} indicator, T-GECO1
517 retains the blue-shifted spectral profile of mTFP1 and its high two-photon cross-section. The
518 results from two-photon imaging in hippocampal slices reveal that these properties can provide a
519 substantial SNR improvement relative to late generation GCaMP variants, particularly for two-
520 photon excitation at 850 nm. We have demonstrated that these properties allow for the reduction
521 of cross-talk in all-optical experiments by reducing the unintended activation of opsins. Other
522 applications that could benefit from the excitability of T-GECO1 at 850 nm could include its
523 combination with red-shifted GECIs or GEVIs to monitor responses from two distinct neuronal
524 populations. Under one-photon excitation conditions, T-GECO1 proved to an effective indicator
525 when measured either in cultured neurons or *in vivo* using fiber photometry.

526 Based on the precedent of the GCaMP series, further engineering and optimization of T-GECO1
527 is likely to provide improved versions that will continue to surpass the GCaMP series under two-
528 photon excitation conditions and may one day rival or surpass the GCaMP series under one-photon
529 excitation conditions.

530

531 **5 Conclusion**

532 T-GECO1 is a high-performance first-generation GECI that is an effective blue-shifted alternative
533 to green and red-emitting indicators like jRCaMP1a or the R-GECO1-derived jRGECO1a,
534 respectively.^{4,10} While further rounds of directed evolution and optimization may be necessary to
535 reach the peak sensitivity and responses of the highly optimized GCaMP series under one-photon
536 excitation, the combination of its teal coloration and high two-photon cross-section make T-
537 GECO1 a practically useful new tool for imaging of dynamic changes in Ca²⁺ concentration using
538 two-photon excitation.

539 **Disclosures**

540 The authors declare no competing interests.

541 **Material and Data Availability**

542 The data supporting this research are available upon request by contacting REC. Plasmid
543 constructs encoding T-GECO1 are available through Addgene or by contacting REC.

544 **Acknowledgments**

545 This work was supported by grants from the Canadian Institutes of Health Research (CIHR, FS-
546 154310 to REC) and the Natural Sciences and Engineering Research Council of Canada (NSERC,
547 RGPIN 2018-04364 to REC). Two-photon characterization work (MD) was supported by the NIH
548 BRAIN grant U24 NS109107 (Resource for Multiphoton Characterization of Genetically-Encoded
549 Probes). Two-photon Ca²⁺ imaging of AP and all-optical data (IB and VE) were supported by the
550 ERC Advanced (Grant ERC-2019-AdG; award no. 885090), the Medical Research foundation
551 FRM (FRM-FDT202204015069) and the Axa research foundation. AA and REC wrote the
552 manuscript. AA, SS, MD, LZ, JZ, S-YW, and YS designed and performed experiments and
553 analyzed the data. IB and VE designed experiments for AP imaging under two-photon excitation

554 and all-optical experiments. IB performed and analyzed the data of the corresponding the
555 experiments. AWL, AGT, VE, KP and REC acquired funding and supervised the project. All
556 authors contributed to editing and proofreading of the manuscript.

557 **References**

- 558 1. R. Y. Tsien, “The green fluorescent protein,” *Annu. Rev. Biochem.* **67**, 509–544 (1998).
- 559 2. T.-W. Chen et al., “Ultrasensitive fluorescent proteins for imaging neuronal activity,” *Nature*
560 **499**(7458), 295–300 (2013).
- 561 3. H. Dana et al., “High-performance calcium sensors for imaging activity in neuronal
562 populations and microcompartments,” *Nat. Methods* **16**(7), 649–657 (2019).
- 563 4. Y. Zhang et al., “Fast and sensitive GCaMP calcium indicators for imaging neural
564 populations,” *Nature* **615**(7954), 884–891 (2023).
- 565 5. L. Zarowny et al., “Bright and High-Performance Genetically Encoded Ca²⁺ Indicator Based
566 on mNeonGreen Fluorescent Protein,” *ACS Sens* **5**(7), 1959–1968 (2020).
- 567 6. O. M. Subach et al., “Novel Genetically Encoded Bright Positive Calcium Indicator NCaMP7
568 Based on the mNeonGreen Fluorescent Protein,” *Int. J. Mol. Sci.* **21**(5), 1644 (2020).
- 569 7. Y. Zhao et al., “Microfluidic cell sorter-aided directed evolution of a protein-based calcium
570 ion indicator with an inverted fluorescent response,” *Integr. Biol.* **6**(7), 714–725 (2014).
- 571 8. Y. Zhao et al., “Inverse-response Ca²⁺ indicators for optogenetic visualization of neuronal
572 inhibition,” *Sci. Rep.* **8**(1), 11758 (2018).
- 573 9. Y. Zhao et al., “An expanded palette of genetically encoded Ca²⁺ indicators,” *Science*
574 **333**(6051), 1888–1891 (2011).
- 575 10. H. Dana et al., “Sensitive red protein calcium indicators for imaging neural activity,” *Elife* **5**,
576 e12727 (2016).

- 577 11. Y. Shen et al., “A genetically encoded Ca²⁺ indicator based on circularly permuted sea
578 anemone red fluorescent protein eqFP578,” *BMC Biol.* **16**(1), 9 (2018).
- 579 12. Y. Qian et al., “A genetically encoded near-infrared fluorescent calcium ion indicator,” *Nat.*
580 *Methods* **16**(2), 171–174 (2019).
- 581 13. Y. Qian et al., “Improved genetically encoded near-infrared fluorescent calcium ion
582 indicators for in vivo imaging,” *PLoS Biol.* **18**(11), e3000965 (2020).
- 583 14. H. Hoi et al., “Highlightable Ca²⁺ indicators for live cell imaging,” *J. Am. Chem. Soc.*
584 **135**(1), 46–49 (2013).
- 585 15. B. F. Fosque et al., “Neural circuits. Labeling of active neural circuits in vivo with designed
586 calcium integrators,” *Science* **347**(6223), 755–760 (2015).
- 587 16. B. Moeyaert et al., “Improved methods for marking active neuron populations,” *Nat.*
588 *Commun.* **9**(1), 4440 (2018).
- 589 17. R. S. Molina et al., “Blue-Shifted Green Fluorescent Protein Homologues Are Brighter than
590 Enhanced Green Fluorescent Protein under Two-Photon Excitation,” *J. Phys. Chem. Lett.*
591 **8**(12), 2548–2554 (2017).
- 592 18. R. Heim, D. C. Prasher, and R. Y. Tsien, “Wavelength mutations and posttranslational
593 autoxidation of green fluorescent protein,” *Proc. Natl. Acad. Sci. U. S. A.* **91**(26), 12501–
594 12504 (1994).
- 595 19. J. Akerboom et al., “Genetically encoded calcium indicators for multi-color neural activity
596 imaging and combination with optogenetics,” *Front. Mol. Neurosci.* **6**(2), 2 (2013).
- 597 20. M. Inoue et al., “Rational Engineering of XCaMPs, a Multicolor GECI Suite for In Vivo
598 Imaging of Complex Brain Circuit Dynamics,” *Cell* **177**(5), 1346–1360.e24 (2019).
- 599 21. F. H. van der Linden et al., “A turquoise fluorescence lifetime-based biosensor for

- 600 quantitative imaging of intracellular calcium,” *Nat. Commun.* **12**(1), 7159 (2021).
- 601 22. M. V. Matz et al., “Fluorescent proteins from nonbioluminescent Anthozoa species,” *Nat.*
602 *Biotechnol.* **17**(10), 969–973 (1999).
- 603 23. H.-W. W. Ai et al., “Directed evolution of a monomeric, bright and photostable version of
604 *Clavularia cyan* fluorescent protein: structural characterization and applications in
605 fluorescence imaging,” *Biochem. J* **400**(3), 531–540 (2006).
- 606 24. T. T. Yang, L. Cheng, and S. R. Kain, “Optimized codon usage and chromophore mutations
607 provide enhanced sensitivity with the green fluorescent protein,” *Nucleic Acids Res.* **24**(22),
608 4592–4593 (1996).
- 609 25. Z. Chen and H.-W. Ai, “Single Fluorescent Protein-Based Indicators for Zinc Ion (Zn^{2+}),”
610 *Anal. Chem.* **88**(18), 9029–9036 (2016).
- 611 26. Y. Qian et al., “A Bioluminescent Ca^{2+} Indicator Based on a Topological Variant of
612 *GCaMP6s*,” *Chembiochem* **20**(4), 516–520 (2019).
- 613 27. R. Tsien and T. Pozzan, “Measurement of cytosolic free Ca^{2+} with *quin2*,” *Methods*
614 *Enzymol.* **172**, 230–262 (1989).
- 615 28. M. Drobizhev et al., “Two-photon absorption properties of fluorescent proteins,” *Nat.*
616 *Methods* **8**(5), 393–399 (2011).
- 617 29. M. Drobizhev, R. S. Molina, and T. E. Hughes, “Characterizing the Two-photon Absorption
618 Properties of Fluorescent Molecules in the 680-1300 nm Spectral Range,” *Bio Protoc.* **10**(2),
619 e3498 (2020).
- 620 30. R. Dalangin et al., “Far-red fluorescent genetically encoded calcium ion indicators,” *bioRxiv*,
621 2020.11.12.380089 (2020).
- 622 31. G. Lopes et al., “Bonsai: an event-based framework for processing and controlling data

- 623 streams,” *Front. Neuroinform.* **9**, 7 (2015).
- 624 32. Y. Nasu et al., “Structure- and mechanism-guided design of single fluorescent protein-based
625 biosensors,” *Nat. Chem. Biol.* **17**(5), 509–518 (2021).
- 626 33. M. Mirdita et al., “ColabFold: making protein folding accessible to all,” *Nat. Methods* **19**(6),
627 679–682 (2022).
- 628 34. Q. Wang et al., “Structural basis for calcium sensing by GCaMP2,” *Structure* **16**(12), 1817–
629 1827 (2008).
- 630 35. A. R. Mardinly et al., “Precise multimodal optical control of neural ensemble activity,” *Nat.*
631 *Neurosci.* **21**(6), 881–893 (2018).